Dead Time-Dependent Line Distortions in Absolute-Value Electron Spin Echo Envelope Modulation Spectra

S. Van Doorslaer, G. A. Sierra, and A. Schweiger

Laboratorium für Physikalische Chemie, Eidgenössische Technische Hochschule, 8092 Zürich, Switzerland

E-mail: schweiger@esr.phys.chem.ethz.ch

It is shown that in pulse EPR experiments, absolute-value spectra can be distorted because of the instrumental dead time to an extent that the interpretation of the spectral features becomes impossible. The mathematical background for the description of the distortions is given, and the far-reaching consequences of the effect are illustrated by model calculations. A cross-term averaging procedure is proposed to get rid of these distortions in two-, three-, and four-pulse electron spin echo envelope modulation experiments. The potential of cross-term averaging is demonstrated in two- and three-pulse experiments on a single crystal and a powder sample. © 1999 Academic Press

Key Words: pulse EPR; dead time–dependent artifacts.

INTRODUCTION

In Fourier transform (FT) spectroscopy such as FT-NMR, pulse EPR, and FT-ion cyclotron resonance, the recorded time-domain signal has to be subjected to a Fourier transformation to get the corresponding spectrum in the frequency domain. Since the instrumental dead time τ_d causes a delay in data acquisition, straightforward Fourier transformation of the data set may lead to distortions of the spectral features. This dead time problem is particularly severe in electron spin echo envelope modulation (ESEEM) spectroscopy (*1*), where, depending on the pulse scheme, the missing portion of the data may correspond to several periods of the resonance frequencies. Various procedures such as linear prediction (*2*) or FT-based algorithms (*3, 4*), have been proposed to reconstruct the data points in the time interval $0 \leq t \leq \tau_d$. After cosine Fourier transformation of the completed data set, a pure absorption spectrum is obtained. In many practical situations, however, the missing time interval is too extended for proper data reconstruction. An alternative approach, which has become very popular in ESEEM spectroscopy, is to Fourier transform the experimentally recorded time-domain data and to compute the absolute-value spectrum.

Since the linewidths in absolute-value spectra are broader than the linewidths in absorption spectra, power spectra, which are distinguished by narrower lines, are sometimes presented.

We, however, consider the use of power ESEEM spectra as a bad habit, since the amplitudes of the peaks no longer reflect the proper line intensities. Apart from the line broadening effect, absolute-value spectra presentations suffer from a much more serious drawback, of which most pulse EPR spectroscopists seem unaware. In multiline spectra with overlapping features, the absolute-value spectra are often heavily distorted by deep holes and large frequency shifts, resulting in splittings that do not really exist and in resonance frequencies that are far from the correct ones. In the ESEEM literature, many examples of strongly distorted absolute-value spectra can be found, which may lead to far-reaching misinterpretations of the data. It was demonstrated earlier that in the case of two lines of equal amplitude and width, the absolute-value spectrum is a function of the relative phase of the two frequencies (*5*). In a hyperfine decoupling study published very recently, it was recognized that resonance lines can manifest in an absolute-value spectrum as holes rather than as peaks (*6*).

In this paper, we give the mathematical background for the description of the dead time-dependent distortions observed in multiline absolute-value spectra and demonstrate by model calculations how tremendous the distortions can be. We then introduce a "cross-term averaging" procedure that allows one to get rid of the distortions, and illustrate the potential of the approach applied in two-, three-, and four-pulse ESEEM experiments.

THEORY AND MODEL CALCULATIONS

We first consider a time-domain signal consisting of a single exponentially damped cosine function which in complex notation is described by

$$s(t) = Be^{i\omega_0 t}e^{-t/\tau}, \quad t > 0 \tag{1}$$

with resonance frequency ω_0 and decay time τ. The complex spectrum

$$S(\omega) = B[A(\omega) - iD(\omega)] \tag{2}$$

consists of the absorption spectrum

$$A(\omega) = \frac{1/\tau}{(1/\tau)^2 + (\omega - \omega_0)^2} \qquad [3]$$

and the dispersion spectrum

$$D(\omega) = \frac{\omega - \omega_0}{(1/\tau)^2 + (\omega - \omega_0)^2}, \qquad [4]$$

with the magnitude or absolute-value spectrum

$$M(\omega) = B\sqrt{A^2(\omega) + D^2(\omega)}. \qquad [5]$$

Considering a dead time τ_d, data acquisition is started at a time $t_0 \geq \tau_d$. The truncated time-domain signal is then given by

$$s_t(t) = B_t e^{i\omega_0 t_0} e^{i\omega_0 t} e^{-t/\tau}, \quad t \geq 0, \qquad [6]$$

with the reduced amplitude $B_t = B e^{-t_0/\tau}$ and the complex factor $e^{i\omega_0 t_0}$ with magnitude 1 and phase $\varphi = \omega_0 t_0$. For the absolute-value spectrum we find

$$M_t(\omega) = \frac{B_t}{B} M(\omega), \qquad [7]$$

which, apart from a reduced amplitude, is identical with the original absolute-value spectrum $M(\omega)$.

Next, we consider a superposition of N exponentially damped cosine functions

$$s(t) = \sum_{n=1}^{N} s_n(t) = \sum_{n=1}^{N} B_n e^{i\omega_0 n t} e^{-t/\tau_n} \qquad [8]$$

that are all in phase at $t = 0$, with amplitudes B_n, frequencies ω_{0n}, and decay times τ_n. Fourier transformation is a *linear* operation, so that the spectrum consists of the sum of the individual lines:

$$S(\omega) = \sum_{n=1}^{N} B_n [A_n - iD_n]. \qquad [9]$$

On the other hand, the computation of the absolute-value spectrum

$$M(\omega) = \left[\sum_{n=1}^{N} M_n^2(\omega) + \sum_{n=1}^{N-1} \sum_{m=n+1}^{N} 2B_n B_m [A_n A_m + D_n D_m] \right]^{1/2} \qquad [10]$$

is a *nonlinear* operation, and Eq. [10] therefore contains *cross-terms* of the form $[A_n A_m + D_n D_m]$.

The truncated signal starting at $t_0 = \tau_d$ is given by

$$s_t(t) = \sum_{n=1}^{N} \frac{B_{tn}}{B_n} e^{i\omega_0 n t_0} s_n(t), \quad t \geq 0 \qquad [11]$$

with $B_{tn} = B_n e^{-t_0/\tau_n}$. For the complex spectrum, we find

$$S_t(\omega) = \sum_{n=1}^{N} B_{tn} e^{i\omega_0 n t_0} [A_n - iD_n], \qquad [12]$$

and the for the absolute-value spectrum we have

$$M_t(\omega) = \left[\sum_{n=1}^{N} \left(\frac{B_{tn}}{B_n} \right)^2 M_n^2(\omega) \right.$$
$$+ \sum_{n=1}^{N-1} \sum_{m=n+1}^{N} 2B_{tn} B_{tm} \cos(\Delta\varphi_{nm})[A_n A_m + D_n D_m]$$
$$\left. + \sum_{n=1}^{N-1} \sum_{m=n+1}^{N} 2B_{tn} B_{tm} \sin(\Delta\varphi_{nm})[A_n D_m - A_m D_n] \right]^{1/2},$$

$$[13]$$

with the phase differences $\Delta\varphi_{nm} = \varphi_n - \varphi_m = (\omega_{0n} - \omega_{0m})t_0$. The square root of the first sum represents the absolute-value spectrum for the case when the peaks are sufficiently well separated from each other. The two double sums represent two types of cross-terms with intensities depending on the phase differences $\Delta\varphi_{nm}$. In both of them the absorptive and dispersive part are mixed together. Note that because of the weighting factors $\cos(\Delta\varphi_{nm})$ the first double sum also contributes to the spectrum recorded with $t_0 = 0$.

To get some deeper insight into Eq. [13], we consider a time-domain signal consisting of two truncated exponentially damped cosine functions, with the absolute-value spectrum

$$M_t(\omega) = \left[\left(\frac{B_{ti}}{B_i} \right)^2 M_i^2(\omega) + \left(\frac{B_{tk}}{B_k} \right)^2 M_k^2(\omega) \right.$$
$$+ 2B_{ti} B_{tk} \cos(\Delta\varphi_{ik})[A_i A_k + D_i D_k]$$
$$\left. + 2B_{ti} B_{tk} \sin(\Delta\varphi_{ik})[A_i D_k - A_k D_i] \right]^{1/2}, \qquad [14]$$

representing the square root of the sum of the two individual power spectra and two cross-terms.

Figure 1 shows the contribution of the cross-terms for $B_{ti} = B_{tk}$, $\tau_i = \tau_k = 1$ μs, $\Delta\varphi_{ik} = 0$ ($t_0 = 0$) (left), $\Delta\varphi_{ik} = 270°$

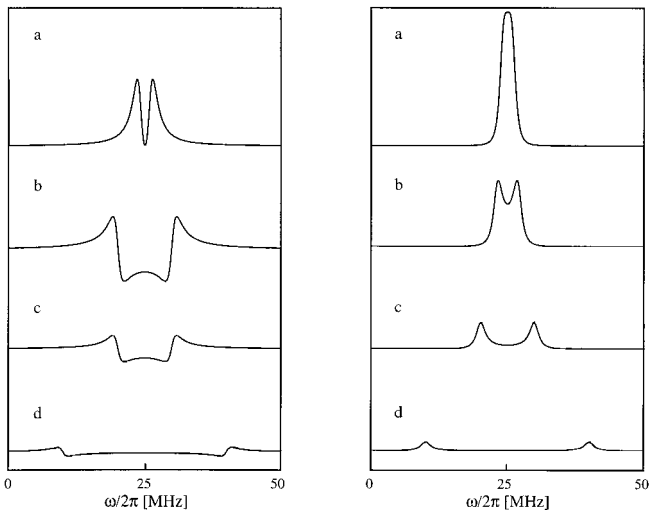**FIG. 1.** Contributions of the two types of cross-terms in Eq. [14] for a two-line spectrum with $B_1 = B_2$, $\tau_1 = \tau_2 = 1$ μs, and frequency differences $\Delta\omega_0/2\pi = 2$ MHz (a), 4 MHz (b), 10 MHz (c), and 30 MHz (d). Left: cross-term $[A_1A_2 + D_1D_2]$, right: $[A_1D_2 - D_1A_2]$. The intensities are normalized to the full amplitude of the power spectrum, which is 1.62 times the height of the spectrum (a) on the right side.

(right), and four different $\Delta\omega_0 = |\omega_{0i} - \omega_{0k}|$ values, $\Delta\omega_0/2\pi = 2$ MHz (a), 4 MHz (b), 10 MHz (c), and 30 MHz (d). As long as the two lines are well separated, $\Delta\omega_0/2\pi \gg 1/\tau_{i,k}$, the influence of the cross-terms is marginal. In the region $\Delta\omega_0/2\pi \approx 1/\tau_{i,k}$, however, the cross-terms can become very intense and their contribution to the individual power spectra, and hence to the absolute-value spectra, is considerable. Depending on $\Delta\omega_0$, τ_i, τ_k, and $\Delta\varphi_{ik}$, the absolute-value spectrum may be distinguished by *deep tapered holes* that often reach the baseline.

Absolute-value spectra can therefore completely be distorted by the cross-terms. Peak maxima may be shifted far away from their proper position and deep holes in the spectrum may mimic splittings that do not exist in reality. This is demonstrated in Fig. 2 on a spectrum consisting of five Lorentzian lines of different frequencies, amplitudes, and widths. In the absorption spectrum shown in Fig. 2a, all five peaks can clearly be recognized. The absolute-value spectrum with $t_0 = 0$ is shown in Fig. 2b. As expected, all the lines are broadened; the resonance frequencies, however, are still clearly indicated by peak maxima and shoulders. Figure 2c shows the absolute-value spectrum recorded with $t_0 = 62$ ns. This spectrum is so severely distorted, in particular by the two deep holes at about 37 and 57 MHz, that most of the observed maxima in the spectrum are no longer related to peak maxima of resonance frequencies.

According to Eq. [13], the amplitudes of the cross-terms are weighted either by $\cos(\Delta\varphi_{nm})$ or $\sin(\Delta\varphi_{nm})$. Since $\Delta\varphi_{nm}$ is a function of time t_0, the contribution of the cross-terms may be averaged to zero by systematically changing time t_0 prior to Fourier transformation, summing up all the power spectra, and

then computing the absolute-value spectrum. The power spectra are not normalized before addition, since this would increase the noise level. This *cross-term averaging procedure* eliminates the spectral distortions so that the correct line positions described by the square root of the first sum in Eq. [13], are restored. This is demonstrated in Fig. 2d, where 11 power spectra with 62 ns $\leq t_0 \leq$ 102 ns and time increments $\Delta t_0 = 4$ ns are added and the absolute-value spectrum is computed. Note that with increasing values of t_0, broad lines tend to disappear. Thus, one has to compromise between the suppres-
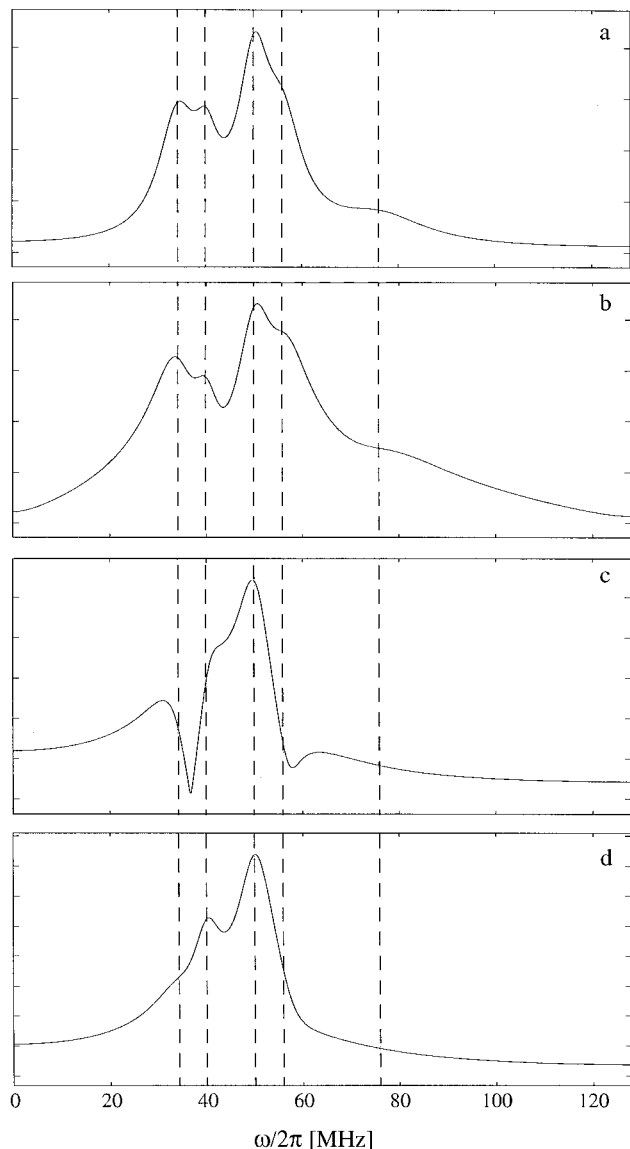

FIG. 2. Spectrum consisting of five Lorentzian lines of different frequencies, amplitudes, and widths. Frequencies $\omega_{0n}/2\pi$: 34, 40, 50, 56, and 76 MHz (dashed lines); damping factors τ_n: 34, 50, 40, 32, 13 μs; amplitudes B_n: 2.6, 1, 3, 2.3, and 1.7. (a) Absorption spectrum. (b) Absolute-value spectrum with $t_0 = 0$ ns. (c) Absolute-value spectrum with $t_0 = 62$ ns. (d) Corresponding absolute-value spectrum after cross-term averaging (summation of 11 spectra with 62 ns $\leq t_0 \leq$ 102 ns and $\Delta t_0 = 4$ ns).

sion of the cross-terms and the loss of broad lines. The best way to find the optimal number of power spectra to be added is by visual control. When the number of power spectra is increased, the cross-term averaged spectrum will first change dramatically (disappearance of the dead time–dependent distortions). At a certain point, the peak positions will no longer alter, but broader lines will gradually disappear.

ABSOLUTE-VALUE SPECTRA IN ESEEM EXPERIMENTS

Since time traces in ESEEM experiments can be described by a sum of damped cosine functions, the procedure introduced in the previous section may directly be applied to get absolute-value ESEEM spectra free of cross-term contributions. In the following, we demonstrate the reconstruction procedure for the two-, three-, and four-pulse ESEEM experiment, and propose additional possibilities for spectral reconstruction for the stimulated-echo-based ESEEM sequence.

All pulse EPR experiments were performed on a Bruker ESP 380E spectrometer at a temperature of 15 K. The two-pulse ESEEM experiments were carried out with $\pi/2$ (π) pulses of length 8 ns (16 ns) for the single crystal sample and 24 ns (48 ns) for the disordered sample with a minimum time interval of 96 ns; 256 data points were sampled with a time increment of 8 ns. For the two-dimensional (2D) three-pulse ESEEM experiments, $\pi/2$ pulses and time increments of length 8 ns were used and a four-step phase cycle was applied (7). The time-domain data were baseline corrected with a suitable polynomial, apodized with a Hamming window, zero filled to 1024 (×1024) data points and Fourier transformed. Further mathematical treatments of the data are discussed later.

Single-crystal experiments were performed on bis(glycinato)copper(II) in triglycine sulfate (8, 9) at arbitrary orientation. As a disordered system, a powder of Co(II)(tetraphenylporphyrin), Co(TPP), in Zn(TPP) as host material has been used.

Two-Pulse ESEEM

The echo amplitude of the two-pulse ESEEM experiment, $\pi/2$–τ–π–τ–echo, of a spin system with $S = \frac{1}{2}$ and $I = \frac{1}{2}$ is given by (10)

$$E(\tau) = 1 - \frac{k}{4}\left[2 - 2\cos(\omega_\alpha\tau) - 2\cos(\omega_\beta\tau)\right.$$
$$\left. + \cos(\omega_+\tau) + \cos(\omega_-\tau)\right], \qquad [15]$$

with the two basic frequencies ω_α and ω_β in the α- and β-manifold of the electron spin, $\omega_+ = \omega_\alpha + \omega_\beta$, $\omega_- = |\omega_\alpha - \omega_\beta|$, and the depth parameter $k = 4\,I_a I_f$, where I_a and I_f denote the transition probabilities of the allowed and forbidden transitions, respectively. If more than one nuclear spin $I = \frac{1}{2}$ couples to the electron spin, the time-domain signal is described by the product rule (10). Since in two-pulse ESEEM the spectral features are usually quite broad and the lines
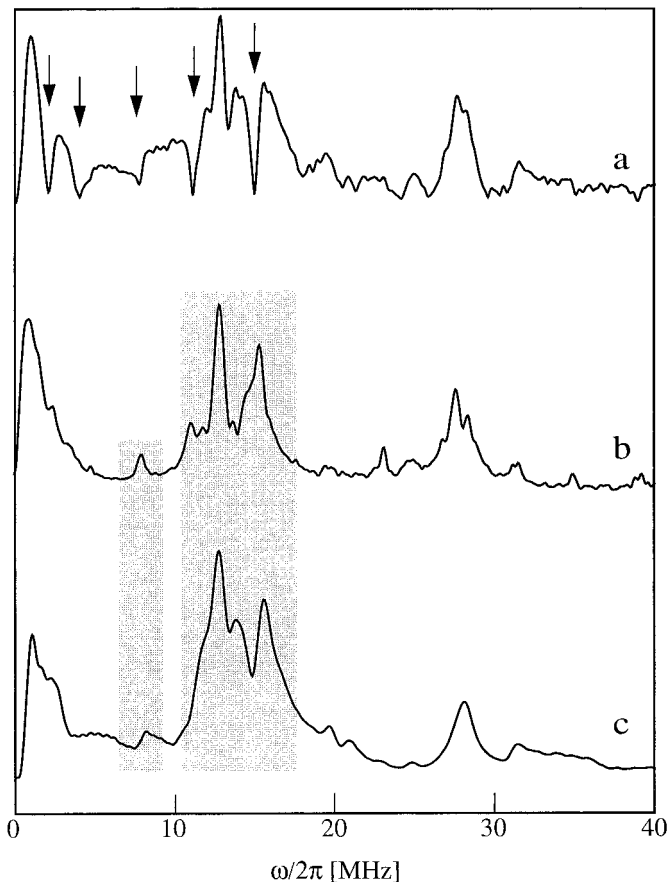

FIG. 3. Two-pulse ESEEM experiments on a single crystal of bis(glycinato)copper(II) in triglycine sulfate (arbitrary crystal orientation, $B_0 = 324$ mT). (a) Absolute-value spectrum, $\tau_0 = 96$ ns (the most pronounced artifact holes are marked by arrows). (b) Corresponding absolute-value spectrum after τ-cross-term averaging (square root of the sum of 100 power spectra with 96 ns $\leq \tau_0 \leq 888$ ns and $\Delta\tau_0 = 8$ ns). (c) Spectrum obtained after Fourier transformation of the corresponding 2D three-pulse ESEEM time-domain data set in the τ dimension and summation of the corresponding absolute-value spectra for variable time T.

overlap, the absolute-value ESEEM spectra reported in the literature are often heavily distorted by the contributions of the cross-terms.

According to Eq. [15], the time-domain trace is represented by a sum of cosine functions that are in phase at $\tau = 0$. The distortions in the absolute-value spectra caused by cross-terms may therefore easily be eliminated by the averaging procedure. Restorations of two-pulse ESEEM spectra are demonstrated in Figs. 3 and 4.

Figures 3a and 3b show single crystal two-pulse ESEEM absolute-value spectra of bis(glycinato)Cu(II) in triglycine sulfate taken at an arbitrary orientation and observer position. The absolute-value spectrum in Fig. 3a is obtained after Fourier transformation of the time-domain signal, recorded with $\tau_0 = \tau_d = 96$ ns. The spectrum is distorted by a number of deep tapered holes (the most pronounced are marked by arrows). The corresponding absolute-value spectrum obtained from the
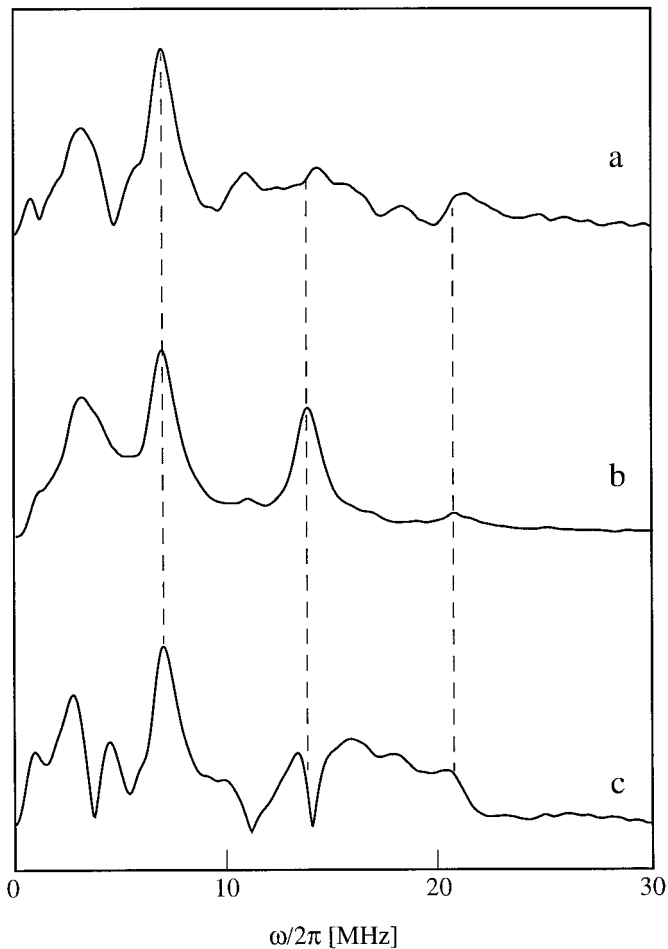
FIG. 4. Two-pulse ESEEM experiment on Co(TPP) in Zn(TPP) powder, observer position $B_0 = 160$ mT. (a) Absolute-value spectrum, $\tau_0 = 96$ ns. (b) Corresponding absolute-value spectrum after τ-cross-term averaging (square root of the sum of 100 power spectra with 96 ns $\leq \tau_0 \leq 888$ ns and $\Delta\tau_0 = 8$ ns). (c) Absolute-value spectrum after linear back-prediction to zero dead time (reconstruction of 12 points) using Ref. (2) with 20 singular values.

same time-domain signal using cross-term averaging (with 96 ns $\leq \tau_0 \leq 888$ ns, in steps of 8 ns) is shown in Fig. 3b. All distortions have disappeared and an absolute-value spectrum with peak maxima that can be considered with confidence as real resonance frequencies is obtained.

Figure 4 demonstrates that absolute-value artifacts also occur in disordered systems. The two-pulse ESEEM absolute-value spectrum of Co(TPP) in Zn(TPP) powder (observer position $B_0 = 160$ mT, corresponding to a proton Larmor frequency of 6.8 MHz) shown in Fig. 4a is obtained after Fourier transformation of the time-domain signal with $\tau_0 = \tau_d = 96$ ns. The corresponding spectrum after cross-term averaging with 96 ns $\leq \tau_0 \leq 888$ ns, in steps of 8 ns, is shown in Fig. 4b. The result is again very impressive. The artificial holes disappear, the troubled base line becomes smooth, and the spectrum is distinguished by well-shaped peaks. Note in particular the peaks at 6.8, 13.6, and 20.4 MHz, which represent

the basic proton frequency and its second and third harmonics, respectively. Figure 4c shows the absolute-value spectrum obtained after linear back-prediction of the time-domain signal to a zero dead time (reconstruction of 12 points) using the method described by Barkhuijsen *et al.* (2). Twenty singular values were taken. It is clear that in this case the linear prediction method fails to reconstruct the exact spectrum.

Both examples clearly demonstrate that in absolute-value ESEEM spectra, the distortions due to the cross-terms are usually by far more serious than the loss of information due to cross-term averaging.

Three-Pulse ESEEM

For the stimulated echo sequence, $\pi/2$–τ–$\pi/2$–T–$\pi/2$–τ–echo, the modulation formula for an $S = \frac{1}{2}$, $I = \frac{1}{2}$ system is given by (10)

$$E(T, \tau) = 1 - \frac{k}{4}\Big[\big[1 - \cos(\omega_\alpha\tau)\big]\big[1 - \cos(\omega_\beta(\tau + T))\big]$$

$$+ \big[1 - \cos(\omega_\beta\tau)\big]\big[1 - \cos(\omega_\alpha(\tau + T))\big]\Big], \quad [16]$$

with a fixed time τ and a variable time T. In three-pulse ESEEM only the basic nuclear frequencies ω_α and ω_β occur. Because of the τ-dependent amplitudes, $(1 - \cos(\omega_\alpha\tau))$ and $(1 - \cos(\omega_\beta\tau))$, the spectra may be distorted by blind spots. Note the similarity between these blind spots and the holes in the absolute-value spectra caused by a delayed data acquisition.

To get rid of the τ-dependence of the signal amplitudes, the three-pulse ESEEM spectra should be taken at several τ values and then summed up. To avoid this time-consuming procedure, the experiment is often carried out with a single τ value for which no blind spots in the frequency region of interest occur. However, this procedure is only justified for the idealized case when data acquisition is started at time $T_0 = -\tau$. According to Eq. [16], a cosine-Fourier transformation will then result in a pure absorption spectrum, although a slight τ-dependent distortion will still be present (see discussion of Fig. 5c).

Even if T_0 is extended to negative values by using a pulse-swapping technique (11), the initial value of T_0 is still limited by the instrumental dead time $T_0 = \tau_d$. The dead time will then again distort the absolute-value spectrum independently of the blind spot behavior. This is demonstrated in Figs. 5a and 5b, which compare the absolute-value spectra of Co(TPP) in Zn(TPP) powder of two three-pulse ESEEM experiments carried out with one and the same τ value ($\tau = 96$ ns corresponding to blind spots at $(10.4)n$ MHz, with $n = 0, 1, 2, \ldots$), but *different* T_0 values (96 and 128 ns). The frequency ranges where the differences in the spectra are most pronounced are marked by gray areas. These T_0-dependent spectral distortions can be removed either by cross-term averaging (T_0-incremen-
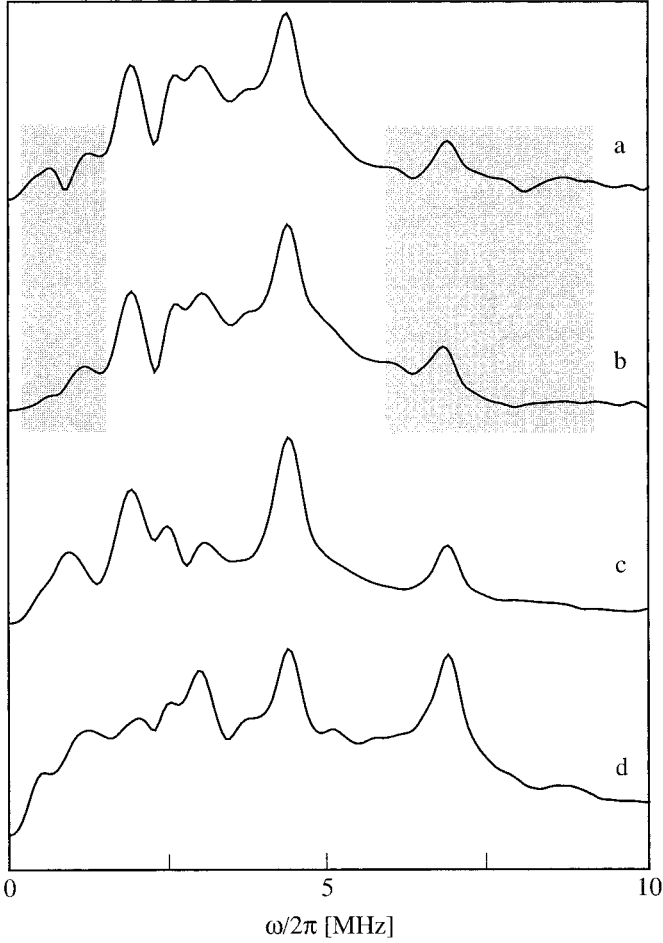
FIG. 5. Three-pulse ESEEM experiment on Co(TPP) in Zn(TPP) powder, observer position $B_0 = 160$ mT. (a) Absolute value spectrum of the three-pulse ESEEM experiment with $\tau = 96$ ns and $T_0 = 96$ ns, (b) $T_0 = 128$ ns. (c) Corresponding absolute-value spectrum after T_0-cross-term averaging (square root of the sum of 100 power spectra with 96 ns $\leq T_0 \leq 888$ ns and $\Delta T_0 = 8$ ns). (d) Absolute-value spectrum obtained after τ-cross-term averaging (96 ns $\leq \tau \leq 600$ ns, in steps of $\Delta \tau = 8$ ns).

tation, Fig. 5c) or by using a reconstruction method (2–4); however, the τ-dependent blind spot behavior remains. By varying τ and summing up the spectra obtained with different τ values, both the τ-dependent and the T_0-dependent distortions are eliminated (Fig. 5d). A comparison of Figs. 5c and 5d shows that even for τ values chosen to shift the blind spots away from the frequency region of interest, the τ-dependence of the modulation amplitudes still leads to spectral distortions.

Note that summation in a second dimension does not necessarily eliminate the dead time–dependent spectral distortions. For example, when the two-dimensional three-pulse ESEEM data set is Fourier transformed in the τ dimension (two-pulse-like spectra) and summed over all T-values, the τ-dependent distortion is not fully averaged out (see terms $(1 - \cos(\omega_{\alpha/\beta} \tau))$ in Eq. [16]). Figure 3 compares the single-crystal absolute-value spectrum of bis(glycinato)copper(II) obtained

in this way (c) with the cross-term averaged two-pulse ESEEM absolute-value spectrum (b). Although the spectrum in Fig. 3c already contains fewer holes than the one shown in Fig. 3a (two-pulse ESEEM without cross-term averaging), obviously not all spectral distortions are eliminated (gray marked areas).

Cross-term artifacts will also occure in two-dimensional spectra obtained by a 2D Fourier transformation. However, the conditions under which holes appear are more complex than in the case of a 1D spectrum and will in general be less severe. Moreover, since in going from a 1D to a 2D spectrum, overlapping lines become better separated from each other, 2D spectra will be less distorted.

Four-Pulse ESEEM

The modulation formula for the four-pulse ESEEM sequence, $\pi/2 - \tau - \pi/2 - t_1 - \pi - t_2 - \pi/2 - \tau -$echo, is given by (12)

$$E(T, \tau) = 1 - \frac{k}{4}(E_I + E_{IIa} + E_{IIb} + E_{IIIa} + E_{IIIb}) \quad [17]$$

with

$$E_I = 3 - \cos(\omega_\beta \tau) - \cos(\omega_\alpha \tau)$$
$$- \sin^2\eta \cos(\omega_+\tau) - \cos^2\eta \cos(\omega_-\tau)$$

$$E_{IIa} = C_\alpha(\tau)\cos[\omega_\alpha(t_2 + \tau/2)] + C_\beta(\tau)\cos[\omega_\beta(t_2 + \tau/2)]$$

$$E_{IIb} = C_\alpha(\tau)\cos[\omega_\alpha(t_1 + \tau/2)] + C_\beta(\tau)\cos[\omega_\beta(t_1 + \tau/2)]$$

$$E_{IIIa} = C_c(\tau)\cos^2\eta[\cos(\omega_\alpha t_1 + \omega_\beta t_2 + \omega_+\tau/2)$$
$$+ \cos(\omega_\beta t_1 + \omega_\alpha t_2 + \omega_+\tau/2)]$$

$$E_{IIIb} = -C_c(\tau)\sin^2\eta[\cos(\omega_\alpha t_1 - \omega_\beta t_2 + \omega_-\tau/2)$$
$$+ \cos(\omega_\beta t_1 - \omega_\alpha t_2 - \omega_-\tau/2)] \quad [18]$$

and

$$C_\alpha(\tau) = \cos^2\eta \cos(\omega_\beta\tau - \omega_\alpha\tau/2)$$
$$+ \sin^2\eta \cos(\omega_\beta\tau + \omega_\alpha\tau/2) - \cos(\omega_\alpha\tau/2)$$

$$C_\beta(\tau) = \cos^2\eta \cos(\omega_\alpha\tau - \omega_\beta\tau/2)$$
$$+ \sin^2\eta \cos(\omega_\alpha\tau + \omega_\beta\tau/2) - \cos(\omega_\beta\tau/2)$$

$$C_c(\tau) = -2\sin(\omega_\alpha\tau/2)\cos(\omega_\beta\tau/2). \quad [19]$$

Several experiments such as DEFENCE (t_1 and τ are kept constant, t_2 is varied) (12), HYSCORE (τ is kept constant, t_1 and t_2 are varied) (12, 13), and the sum peak experiment ($t_1 = t_2$ is varied, τ is either kept constant (1D) or varied (2D)) (14, 15) are based on this pulse sequence.

For the 1D DEFENCE experiment, it has already been recognized (12) that there will be suppression effects due to the t_1 and τ dependence of the echo modulation amplitudes, Eqs.

[18] and [19]. These effects can virtually (but not fully) be eliminated by an appropriate choice of t_1 and τ. Equation [18] shows that also the dead time t_{2d} of the second free evolution period has to be considered. All the suppression effects occurring in a DEFENCE experiment can be removed by cross-term averaging with respect to the time interval τ (see Eqs. [18] and [19]).

In HYSCORE spectra, spectral distortions depend not only on the pulse spacing τ, but also on the two dead times t_{1d} and t_{2d}. From Eqs. [18] and [19], it can be seen that an addition of HYSCORE spectra with different τ values will again remove all dead time–dependent distortions. In practice, however, instrumental limitations often make such three-dimensional HYSCORE experiments (*16*) very demanding and time consuming. Therefore, one always has to keep in mind possible dead time–dependent distortions in the interpretation of HYSCORE spectra taken at one τ value.

CONCLUSIONS

It has been shown that severe line distortions occur in absolute-value spectra obtained after Fourier transformation of a truncated signal. In pulse EPR, truncation of the recorded time-domain signal is caused by the instrumental dead time. The origin of the distortions can be put down to the fact that the absolute-value spectrum depends on the relative phase of the different frequencies contributing to the time-domain signal.

The consequences of these dead time–dependent effects are discussed for two-pulse, three-pulse, and four-pulse absolute-value ESEEM spectra. Examples of heavily distorted ESEEM spectra are shown for both a single-crystal and a disordered system. In these spectra, splittings that do not exist and reso-nance frequencies that are far from the correct ones are observed. In order to get rid of the artifacts, a cross-term averaging method is proposed. Additional possibilities for spectral reconstruction are given for the three- and four-pulse ESEEM sequences.

REFERENCES

1. S. A. Dikanov and Yu. D. Tsvetkov, "Electron Spin Echo Envelope Modulation (ESEEM) Spectroscopy," CRC Press, Boca Raton (1992).

2. H. Barkhuijsen, R. de Beer, W. M. M. J. Bovée, and D. van Ormondt, *J. Magn. Reson.* **61,** 465 (1985).

3. W. B. Mims, *J. Magn. Reson.* **59,** 291 (1984).

4. A. V. Astashkin and A. Kawamori, *J. Magn. Reson. A* **112,** 24 (1995).

5. J. P. Lee and M. B. Comisarow, *J. Magn. Reson.* **72,** 139 (1987).

6. G. Jeschke and A. Schweiger, *J. Chem. Phys.* **106,** 9979 (1997).

7. C. Gemperle, G. Aebli, A. Schweiger, and R. R. Ernst, *J. Magn. Reson.* **88,** 241 (1990).

8. J. Stankowski, A. Wieckowski, and S. Hedewy, *J. Magn. Reson.* **15,** 498 (1974).

9. R. Böttcher, D. Heinhold, and W. Windsch, *Chem. Phys. Lett.* **49,** 148 (1977).

10. W. B. Mims, *Phys. Rev. B* **5,** 2409 (1972).

11. J. M. Fauth, A. Schweiger, L. Braunschweiler, J. Forrer, and R. R. Ernst, *J. Magn. Reson.* **66,** 74 (1986).

12. A. Ponti and A. Schweiger, *J. Chem. Phys.* **102,** 5207 (1995).

13. P. Höfer, A. Grupp, H. Nebenführ, and M. Mehring, *Chem. Phys. Lett.* **132,** 279 (1986).

14. A. Schweiger, *Angew. Chem. Int. Ed. Engl.* **30,** 265 (1991).

15. S. Van Doorslaer and A. Schweiger, *Chem. Phys. Lett.* **281,** 297 (1997).

16. P. Höfer, *J. Magn. Reson. A* **111,** 77 (1994).